JOURNAL OF APPLIED ELECTROCHEMISTRY 14 (1984) 15–22

Distribution of reaction in a cell with gas-evolving electrodes. I. Magnesium/silver chloride seawater battery

R. E. W. JANSSON*, R. J. MARSHALL

Chemistry Department, Southampton University, Southampton, UK

Received 21 January 1983

The effects of gas evolution on the distribution of reaction at high current densities have been studied experimentally in a model Mg–AgCl battery cell. Measurements of current, potential, pH and temperature were made at four vertical locations during discharge at applied pressures between 1–6 bar (g). Temperature and pressure were found to influence local current density with consequences for overall battery lifetime.

1. Introduction

Flow visualization [1] and marker experiments [2] have shown that gas bubbles can profoundly affect the structure of the flow in a cell. While creditable attempts have been made to model the effects of bubbles on mass transport [3–6] and current distribution [7], the models are not yet powerful enough to deal with many practical cases, and there is justification for qualitative experiments to define the dimensions of the interaction between heterogeneous reaction, homogeneous reaction and bubble evolution.

An excellent example of this problem in acute form is the reaction environment in the magnesium–silver chloride seawater battery [8]. In high-drain applications of this cell the nominal current density is typically 400 mA cm^{-2}, with only slow recirculation of the seawater electrolyte (Reynolds number, $Re \cong 50$). By-products of the anode reaction

$$Mg \longrightarrow Mg^{++} + 2e$$

are hydrogen gas [11] and complex oxychlorides and hydroxides of magnesium and the alloying metals, e.g. lead and zinc, which are incorporated to increase the anode voltage [9]. To a first approximation the solid residues ('sludge' in battery jargon) can be though of as magnesium hydroxide, although the actual composition depends critically on the conditions and initial composition of the anode (see Table 1). One common failure mode of seawater batteries is associated with the blockage of the flow channel with sludge [10].

The cathodic reaction

$$2AgCl + 2e \longrightarrow 2Ag + 2Cl^-$$

gives a spongy matrix of silver through which liberated chloride anions diffuse into the bulk flow.

As the batteries are normally run with a high degree of recycling, the composition of the electrolyte varies with time and also with distance along the battery plate. The temperature also varies with time and distance. The void fraction of bubbles increases along the length of the plate. In fact, the void fraction and the increasing conductivity due to the liberation of Mg^{++} and Cl^- and increasing temperature work in opposite senses, so that it is extremely difficult to predict the inter-electrode *iR* drop, hence the distribution of reaction under constant current conditions. Further, the battery is intended to work at a variety of depths (pressures) which also affects the void fraction. Clearly, the system is extremely interactive and the usual battery models, based on resistive networks, are inadequate to predict failure modes in many cases.

* Present address: Monsanto Company, St. Louis, Missouri 63167 USA.

0021–891X/84 $03.00 + .12.

Table 1. Per cent composition (by weight) of the metal content of the magnesium alloys, the sludge deposit and spent electrolyte, determined by atomic absorption spectroscopy†

System	*Location*	*Mg*	*Al*	*Zn*	*Pb*
Anode Alloy					
AZ61*		93	6	1	–
20–40° C	Deposit at top of plate	93.6	5.1	1.3	–
	Deposit at bottom of plate.	96.4	2.9	0.6	–
	Spent electrolyte.	99.7	0.1	0.003	–
Anode Alloy					
AP65*		89	6	–	5
22–46° C	Black deposit.	79.4	8.7	–	11.8
	White deposit.	98.8	2.3	–	3.9
	Spent electrolyte.	99.96	0.0	–	0.04

* Manufacturers data.
† Mg, Zn, Pb on Varian Techtron 1100.
† Al on Varian A.A.5. (Flameless.)

Experiments were carried out across a wide range of conditions to assess the sensitivity of the performance of the battery to the conditions and to gain insight into the general problem of high rate reactions in the presence of bubble evolution.

2. Experimental details

Experiments were performed at applied pressures of from zero to six bar with synthetic seawater as electrolyte (i.e. 23.5 g dm^{-3} NaCl + 5 g dm^{-3} $MgCl_2$ + 3.9 g dm^{-3} Na_2SO_4 + 1.1 g dm^{-3} $CaCl_2$ + 0.66 g dm^{-3} KCl + 0.19 g dm^{-3} $NaHCO_3$) at an initial temperature of 30 to 50° C. To simplify the interpretation of results, a once-through flow system was used, Fig. 1. Gases evolved during discharge were allowed to escape through a relief valve set to the operating pressure. Connections between the pipes were made with Legris series 2000 snap fittings.

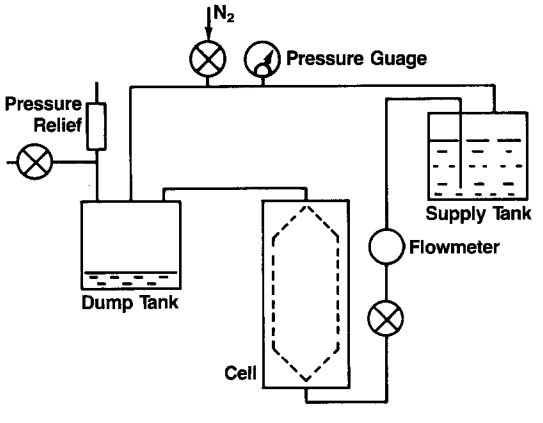

Fig. 1. Flow circuit.

Diagrams of the cell are shown in Figs. 2 and 3. The AgCl plate was split into four sections so that the currents in different segments could be recorded. Temperature, pH and cathode potential (vs a AgCl reference electrode) in each segment were also recorded. Figure 3 shows the mechanical construction of the cell and its backplates, which were made from 9 mm thick aluminium plate. The notches in the backplates for the through bolts allowed rapid (~ 1 min) disassembly of the cell for inspection of the electrodes at the end of each run. The interelectrode gap was maintained at 0.5 mm by 1 mm diameter glass beads embedded in a square array to half their depth in the AgCl, a design feature of the commercial plates employed. Torquing the tie bolts always to 0.5 kg m avoided stress deformation of the acrylic cell formers and also provided reproducible cell gap and contact resistance with the foil current collectors (Fig. 3).

A 16-channel amplifier was constructed to condition the analog signals from within the cell (4 currents, 4 cathode potentials, 4 temperature and 4 values of pH), a major design requirement being the avoidance of cross-tracking since a common electrolyte and single output ground were shared by all the probes and the cell itself [12]. The high impedance of the pH probe membranes made this

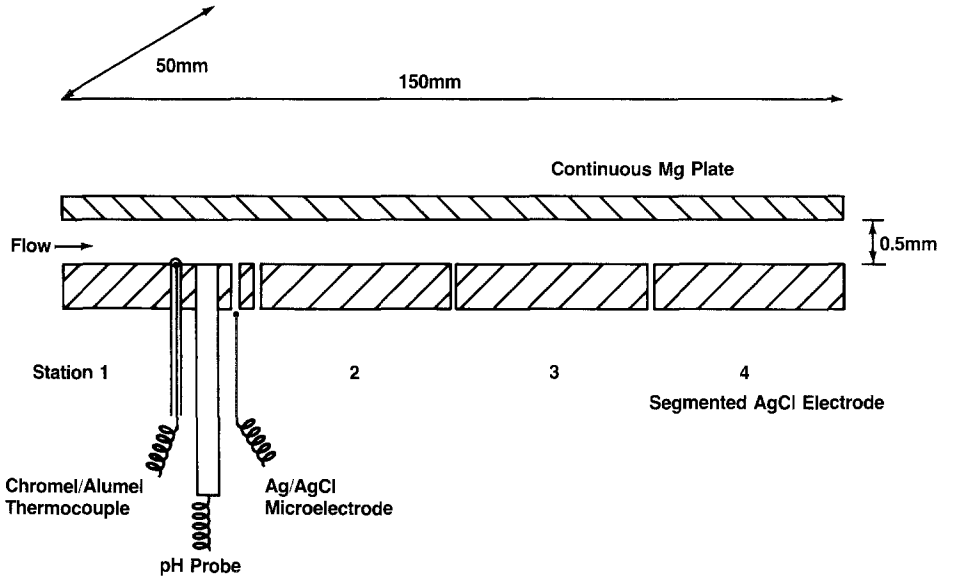

Fig. 2. Schematic diagram of instrumented battery plates (not to scale).

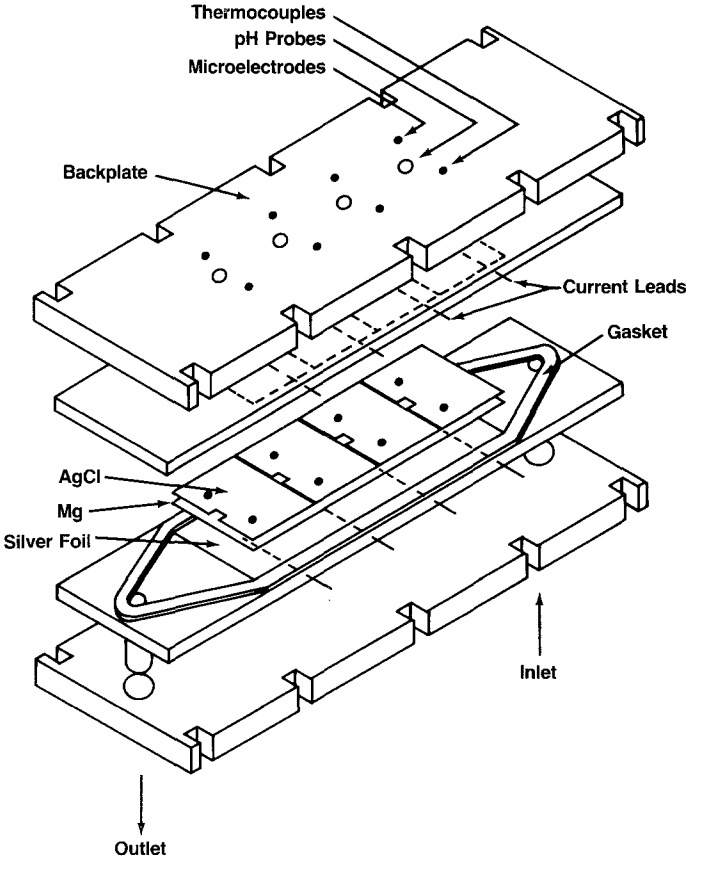

Fig. 3. Construction of cell.

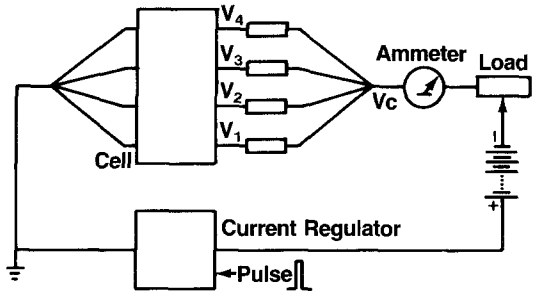

Fig. 4. Electrical discharge circuit.

problem particularly acute, but the use of optical isolators and high impedance differential amplifiers circumvented this problem [1, 10].

The cell was discharged at 30 A constant current (nominally, 400 mA cm^{-2}) through a solid state current regulator, Crompton Universal Ammeter, rheostat load resistor and lead acid battery power supply. The current in each segment of the cell under test was monitored via the voltage across a 0.01 Ω heavy duty series resistor made from Ni–chrome wire. The four resistors were balanced to within 5% of each other by filing notches in the wire.

Voltages across the load resistors were monitored continuously, each load resistor and amplifier having first been calibrated, to give the segment currents, the sum of which always agreed with the total cell current, measured by ammeter, to within 5%. The overall cell voltage was taken between the common point, V_c, and ground (Fig. 4).

The strong potential gradient normal to the electrode surface (typically 1000 mV per mm) makes it difficult to place potential probes in the solution reproducibly, therefore the probes were sited behind small holes in the AgCl macro-electrode (Fig. 2). The microelectrodes were made by dip coating the tip of a 0.4 mm diameter silver wire in molten silver chloride. Of course, the potential measured was a function of free chloride ion in the electrolyte, and therefore changed with time, but this drift was small compared with the large potential difference caused by exhaustion of the AgCl electrode.

Chromel/alumel thermocouples mounted inside 1 mm welded PVC insulating sleeves were set in the cell with their ends flush with the AgCl surface. A water/ice mixture was used as the cold junction reference temperature.

Small, flat ended combination pH probes of a geometry capable of operation at pressure were not available, so a set of combination probes was made from pH glass blanks supplied by EIL Ltd. (Fig. 5). The inner reference electrode was a silver wire tipped with AgCl in a 4 mol dm^{-3} solution of KCl buffered to pH 4.0 with potassium hydrogen phthalate. The external reference was a silver foil which had been wrapped around the glass barrel of the probe and anodized in 1 mol dm^{-3} HCl to produce an AgCl coating. This foil also served as electrical screening for the pH probe. A glass cloth sleeve saturated with KCl extended to the tip of the probe, and, when held tightly in place with a polyolefin heat shrunk outer covering, this provided a void-free salt bridge which minimized contamination of the reference electrode by seawater under pressure. The overall diameter of the combination pH/potential probe was 5 mm.

Each pH probe was connected to a high impedance (10^{12} Ω MOSFET) d.c. amplifier which, with its own power supply and an optical isolator on the output stage, was able to operate floating electrically from the rest of the system. To eliminate sensitivity to electric field gradients between the glass membrane and external reference, each pH meter was operated in conjunction with a dual pulse generator connected to the cell current regulator. Within the interval of a pulse which electronically switched the cell current to zero, a second pulse operated a sample and hold device which read and stored the output voltage of the pH meter amplifier. The length of each pulse and the delay between them were arranged so that the cell current transient effects were not sensed. The

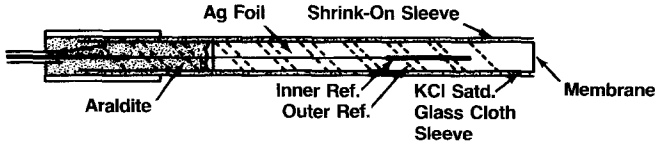

Fig. 5. Combination glass pH electrode.

overall sampling frequency was 3 Hz which, with a pulse length of 300 μs, gave a mark-space-ratio of 1:1000 so that the measurement did not significantly affect the discharge of the battery, hence its internal chemical composition.

The 16 amplifier outputs, together with the cell voltage, V_c, and flow meter signal were input to a 20 channel home-built multiplexer, a sequential sampling rate of 20 Hz giving an effective sample rate per channel of 1 Hz, the internal clock of the multiplexer, accurate to 0.0005 Hz, serving as the time base for the experiment. The multiplexer output plus a synchronising signal were recorded on a Racal Store 4 data tape recorder for later play-back to a PDP 11/50 data analysis computer. This was found to be a more secure form of data capture than direct acquisition of multi-channel information by the time sharing computer.

In the discharge experiments themselves, pressure was established and the electrolyte flow through the cell adjusted to a nominal 80 $cm^3 min^{-1}$. The cell current was then switched on simultaneously with the data acquisition system. Discharge time varied from two to five minutes depending on operating conditions. At the end of each run the pH probes were removed from the cell and the pH meters calibrated against BDH buffers (BS 1647:1961) at pH 8.0, 9.0 and 10.0. Approximately 25 discharges were run under a variety of conditions.

3. Results and discussion

Figure 6 shows the variation of current density in the cell at various pressures with entry seawater at 30° C. The high local current density at station 1 is probably partly due to entry effects. Due to accumulation of bubbles in the electrolyte the current decreases towards the top of the cell at low pressure, but as the pressure increases this trend is inverted until at 6 bar the current density increases towards the top of the plate, i.e. at this pressure it is the increasing concentrations of Mg^{++} and Cl^- which principally influence the current distribution. However, at 30° C, the two effects are almost balanced over the whole pressure range since the variation is only ± 5% of the mean.

In contrast, Fig. 7 shows the distribution of current density, with electrolyte delivered at 50° C. The distribution of current is highly non-uniform, about 25% less current flowing in the top portion of the cell, compared to the bottom, at 1 bar, with a marked pressure dependence. The effect is caused by an increase in hydrogen volume in the system at the higher temperature, and the current distribution is dominated by the presence of the gas until the effect of increasing ionic strength just begins to reverse the trend at 6 bar. It is interesting to note that a current minimum appears which is insensitive to pressure, and this shifts, from station 2 in the low temperature case towards the top of the cell as the temperature is increased. The direction of this shift is in accordance with a change from ionic strength to gas voidage as the stronger factor controlling the current distribution.

The operating temperature not only has an effect on current distribution, but also on the failure mode of the cell. With seawater entering the cell at 30° C, electrolyte flow persisted until the

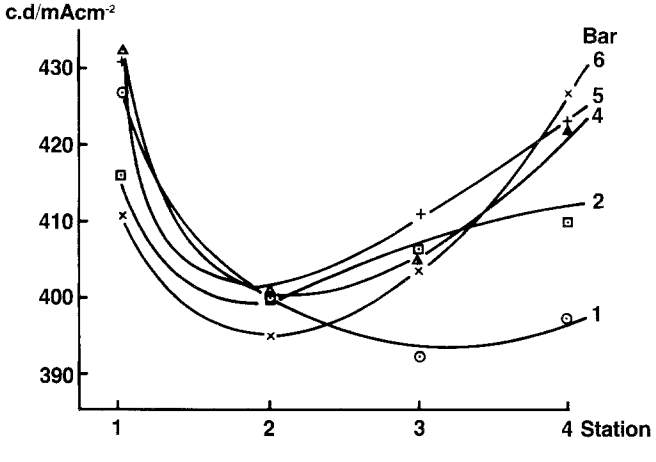

Fig. 6. Current density distribution, 30° C entry seawater.

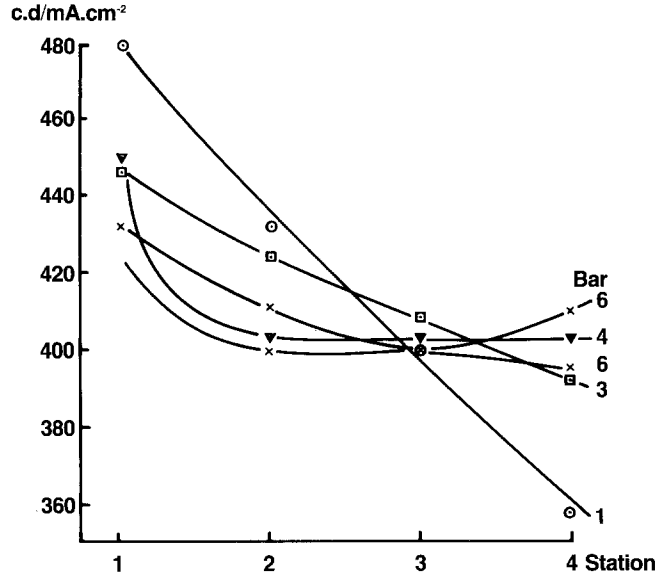

Fig. 7. Current density distribution 50° C entry seawater.

end of discharge, which was indicated by a rapid decline in cell voltage. Figure 8a shows that each segment current was maintained at a steady level until a rapid rise was seen in cathode polarization, indicating exhaustion of the silver chloride. Since under constant impressed current conditions, any drop in current at one location forces a rise elsewhere, it can be seen that failure propagated in a cascade fashion from the bottom to the top of the cell, i.e. away from the highest current density region.

In all of the higher temperature discharges electrolyte flow halted spontaneously quite early on in the run. Figure 8b shows that the segment current levels gradually converge to a point, after which they become unsteady and diverge rapidly. The termination of electrolyte flow occurred simultaneously with the onset of divergence. A drop in current at station 1 forced a rise at station 4, i.e. in this case the catastrophe was initiated at the bottom of the cell and swept upwards, but this event was not associated with a sudden rise in cathode overpotential as observed in the lower temperature cases. Therefore in the high temperature cases the failure was not due to early cathode exhaustion, but blockage of the channel by reaction products. For magnesium anodes the rate of hydroxide formation is proportional to the current density (the so called 'negative difference' property of magnesium [9]) and in the example shown (at 2 bar) it was the bottom segment, where the current density was highest, which failed first. Thus although the distribution of reaction was determined principally by the local void fraction, the onset of catastrophe was determined by the temperature via the local kinetics of formation of the hydroxide/oxychloride sludge. The high proportions of alloying metals found in this material (Table 1) suggest that the chemistry is highly complex.

Although local in its origin, the result of stagnant electrolyte was seen throughout the cell as a temperature increase plus an initial rise in cell voltage, which is soon followed by a premature collapse. This behaviour was seen at all pressures between 1–6 bar, and the shortened run time left the AgCl cathode significantly under-utilized, Fig. 9. Not surprisingly, the effects of unequal current distribution are reflected most strongly in the low pressure data, although operating temperature is still the dominant factor.

The pH data turned out to be rather uninteresting, steady state values between 6.5 and 8.5 being observed at all stations just prior to closing of the gap by sludge or exhaustion of the cathode. This suggests that the bulk OH^- concentration obtained in the course of a discharge did not markedly influence the kinetics of the electrochemical or chemical reactions of the electrode materials. That the sludging material grew as a sponge on the anode surface rather than accreted by precipitation from the bulk of the electrolyte, was also

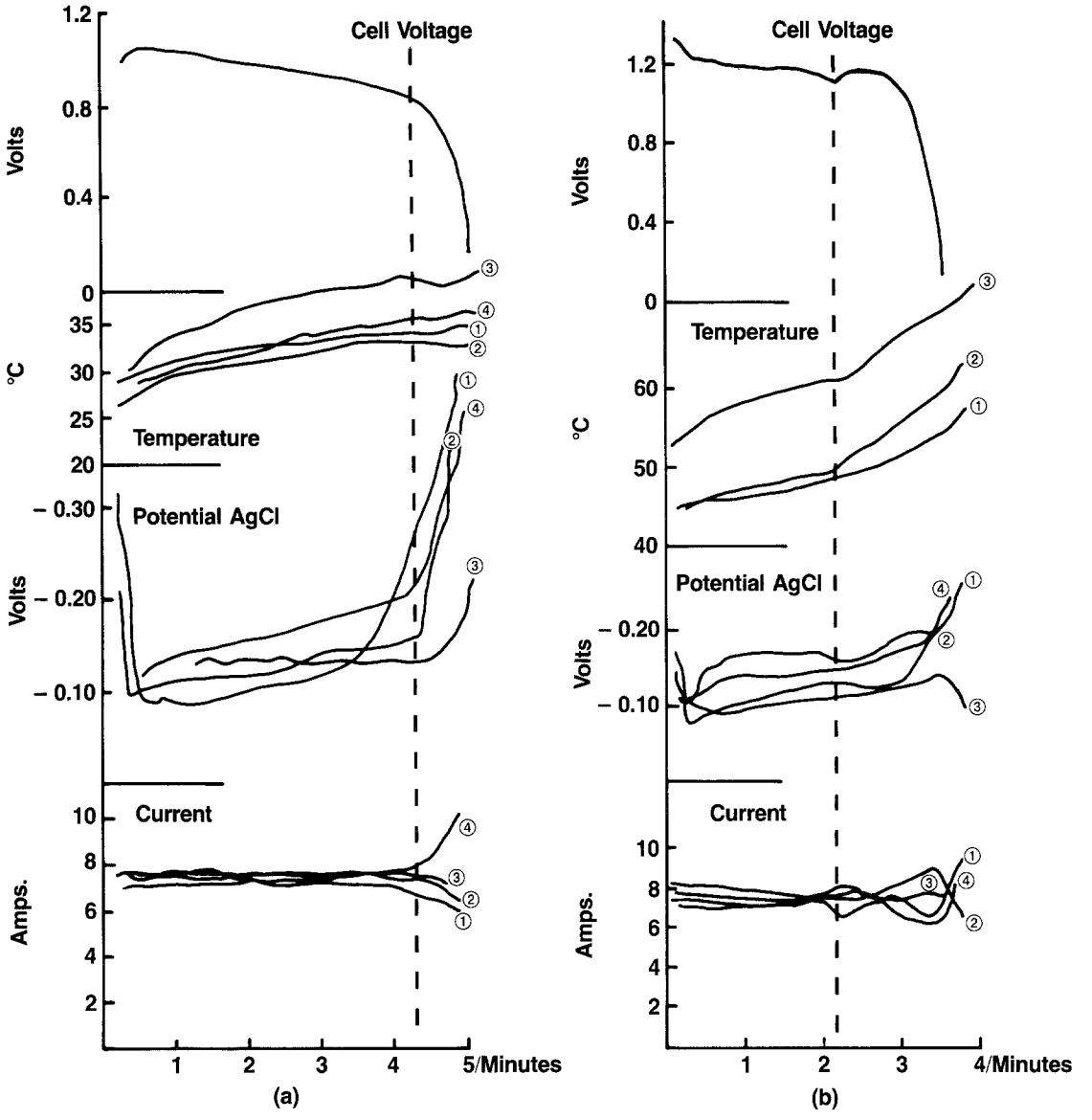

Fig. 8. Local condition during cell discharge, AP65 anode 2 bar (g): Duration limited by (a) normal exhaustion of AgCl electrode and (b) early failure due to cell gap sludging.

indicated by visual inspection of the failed plates after these experiments.

4. Conclusions

Two markedly different modes of behaviour have been observed. In one case a smooth discharge was obtained until exhaustion of the depolarizer material; in the other, a local build up of solid reaction products initiated an unstable condition via stoppage of the flow which caused early failure of the whole cell. The rate of formation of hydrogen and anodically generated products was increased by a rise in temperature and was also proportional to the anodic current density. When the local current densities became so high that growth of hydroxide/oxychloride sludge exceeded its rate of removal by convective forces in the electrolyte then the cell gap became blocked and failure occurred. In a cell-pile, the blocked cell is

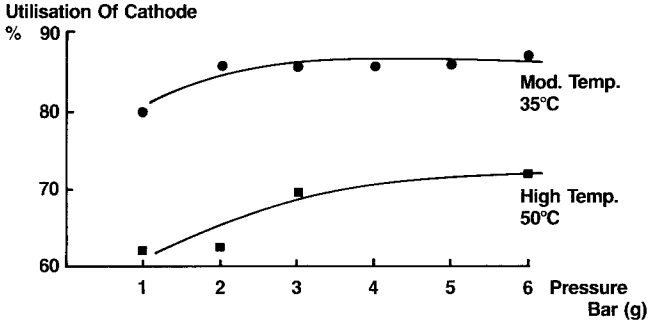

Fig. 9. Cathode utilization as a function of pressure.

driven electrically by all the other cells, leading to catastrophe.

Before failure, the distribution of reaction is influenced both by the void fraction of bubbles (hence the operating pressures) and the conductivity of the electrolyte, which depends on the ionic products of reaction. In practical cases, where most of the electrolyte is recycled, the instantaneous behaviour therefore depends on the integral over time of all the past behaviour, so it is not surprising that it is difficult to model the system with electric circuit analogues.

Although the low Reynolds number, high current density conditions are unusual for an electrochemical (synthesis) reactor, a general point is illustrated; constant current electrolysis accompanied by gas evolution can create local conditions which deviate markedly from the design conditions, leading to loss of selectivity and passivation or corrosion of the electrode. This is potentially a problem where large vertical electrodes are used, particularly if high conversion in a single pass is required.

Acknowledgement

This work was carried out with the support of the Procurement Executive, Ministry of Defence, to whom we are grateful.

References

[1] R. J. Marshall, PhD thesis, Southampton University (1981).
[2] R. E. W. Jansson and R. J. Marshall, *Electrochim. Acta* **27** (1982) 823.
[3] N. Ibl, *ibid.* **24** (1979) 1105.
[4] H. Vogt. *ibid.* **23** (1978) 203.
[5] L. J. J. Janssen and S. J. D. Van Stralen, *ibid.* **20** (1981) 1011.
[6] C. I. Elsner and S. L. Marchiano, *J. Appl. Electrochem.* **12** (1982) 735.
[7] C. W. Tobias, *J. Electrochem. Soc.* **106** (1959) 833.
[8] D. T. Sharpe, US Patent 3005864 (1945).
[9] R. Glicksman, *J. Electrochem. Soc.* **106** (1959) 83.
[10] D. W. Faletti and L. F. Nelson, *Electrochem. Technol.* **3** (1965) 98.
[11] J. L. Robinson and P. F. King, *J. Electrochem. Soc.* **108** (1961) 36.
[12] J. Overstall and R. E. W. Jansson, *J. Chem. Tech. Biotechnol.* **30** (1980) 313.